MRS BULLETIN

Serving the International Materials Research Community

A Publication of the Materials Research Society

February 2007, Volume 32, No. 2

Functional Nanowires

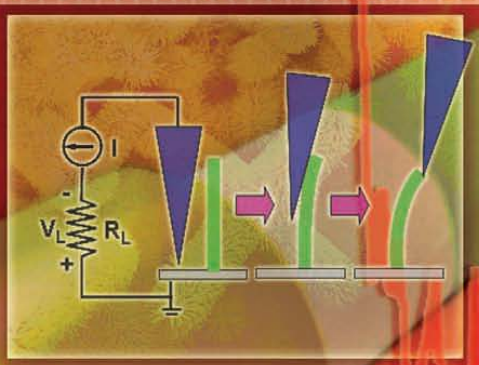

Also in This Issue:

The Mechanics and Physics of Defect Nucleation

Piezoelectric Nanostructures: From Growth Phenomena to Electric Nanogenerators

Zhong Lin Wang

Abstract

Zinc oxide is a unique material that exhibits semiconducting, piezoelectric, and pyroelectric multifunctionalities. By controlling the size and orientation of the polar surfaces of ZnO nanobelts, single-crystal nanocombs, nanorings, nanohelices, nanosprings, and nanobows of ZnO have been synthesized. This article centers on the fundamental growth mechanism and fabrication of electromechanical devices based on piezoelectric ZnO nanostructures, including a nanogenerator using aligned ZnO nanowires for converting nanoscale mechanical energy into electric energy. The mechanism of the electric nanogenerator relies on the unique coupling of the piezoelectric and semiconducting properties of ZnO, which is the fundamental principle of nano-piezotronics, a new field using the piezoelectric effect for fabricating electronic devices and components. The approach has the potential of converting biological mechanical energy, acoustic/ultrasonic vibration energy, and biofluid hydraulic energy into electricity, demonstrating a new pathway for self-powering of wireless nanodevices and nanosystems.

Introduction

Since the first synthesis of oxide nanobelts in 2001,[1] research in functional oxide-based one-dimensional (1D) nanostructures has rapidly expanded due to their potential applications in optics, optoelectronics, catalysis, and piezoelectricity. Semiconducting oxide nanobelts are a unique group of quasi-1D nanomaterials that have been systematically studied for a wide range of materials with distinct chemical compositions and crystallographic structures.[2] Field-effect transistors[3] and ultrasensitive nano-sized gas sensors,[4] as well as nanoresonators[5] and nanocantilevers,[6] have been fabricated based on individual nanobelts. Thermal transport along nanobelts has also been measured.[7]

Zinc oxide (ZnO) is a material that has diverse nanostructures. Owing to its noncentral symmetry, ZnO is not only semiconducting but also piezoelectric and pyroelectric. ZnO is a versatile smart material that has key applications in catalysts, sensors, piezoelectric transducers,[8] transparent conductors,[9] and surface acoustic wave devices.[10] The structure of ZnO can be described as a number of alternating planes composed of tetrahedrally coordinated O^{2-} and Zn^{2+} ions stacked along the *c*-axis (Figure 1a). The oppositely charged ions produce positively charged Zn(0001) and negatively charged O(000$\bar{1}$) polar surfaces, resulting in a normal dipole moment and spontaneous polarization along the *c*-axis (Figures 1a and 1b). If the elastic deformation energy is largely suppressed by reducing the thickness of a nanobelt, the polar nanobelt could self-assemble into different shapes, such as a nanospring (Figure 1c), by minimizing the electrostatic energy coming from the ionic charges on the polar surfaces.[11] The existence of polar charges on the basal plane is the driving force for forming nanorings[12] and nanohelices, which could be candidates for nanoscale transducers, actuators, and sensors.

Nanosprings and Nanorings

A wide range of nanostructures of ZnO have been synthesized (Figure 2) by controlling the growth kinetics, local growth temperature, and chemical composition of the source materials using a solid-state thermal sublimation process.[13,14] The key for the formation of these novel configurations is the existence of large-area polar surfaces. Controlling the pre-growth chamber pressure was found to be the key for the stability of the polar surface and high-yield synthesis.[15] Taking the nanospring shown in Figure 2d as an example, the ZnO nanobelt grows along [2$\bar{1}\bar{1}$0] (the *a*-axis), with its top/bottom surfaces $\pm$(0001) and the side surfaces $\pm$(01$\bar{1}$0). Due to the small thickness of 5–20 nm and large aspect ratio of ~1:4, the flexibility and toughness of the nanobelts are extremely high.[16]

The formation of the nanosprings can be understood from the nature of the polar surfaces. If the surface charges are uncompensated during growth, the spontaneous polarization induces electrostatic energy due to the dipole moment; rolling up to form a circular ring minimizes the overall dipole moment, reducing the electrostatic energy. On the other hand, bending the nanobelt produces elastic deformation energy. The stable shape of the nanobelt is therefore a compromise that minimizes the total energy contributed by spontaneous polarization and elasticity. The electrostatic repulsive force between two successive rings of a nanobelt leads to the formation of a nanospring as growth continues.[11]

By introducing impurities such as indium into the raw materials, we have synthesized a seamless nanoring of ZnO (Figure 2e).[12,17] The indium introduces planar defects that tend to reduce the energy of the polar surface, making it easier to form a seamless nanoring. The scanning electron microscopy (SEM) image (Figure 2e) recorded at high magnification clearly shows the uniform circular shape and flat surfaces of the complete ring. Transmission electron microscopy (TEM) indicates that the nanoring is a single crystal

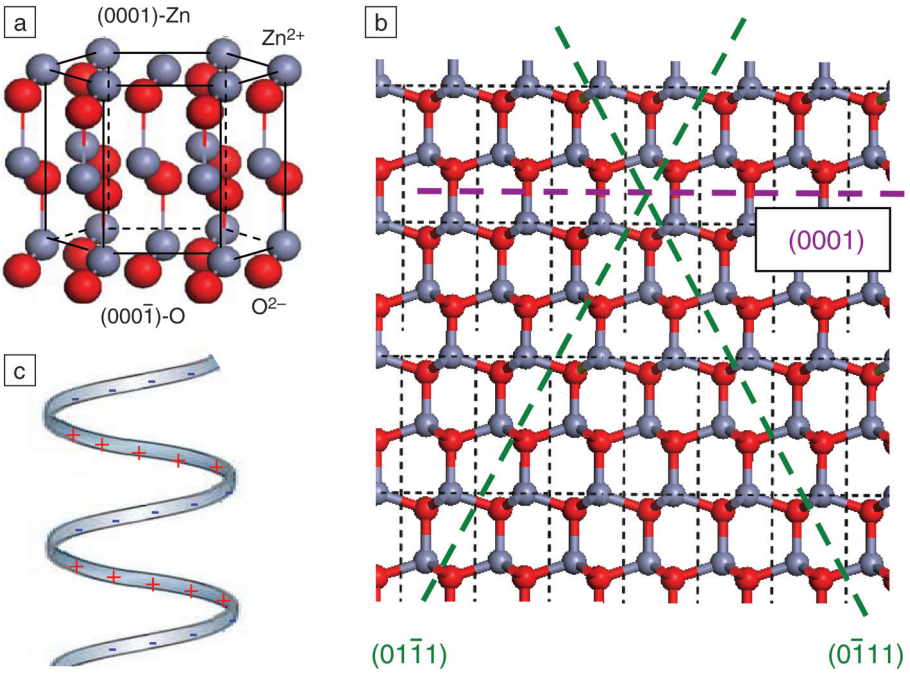

Figure 1. (a) Wurtzite structure model of ZnO. The tetrahedral coordination of Zn-O is shown. (b) Structure model of ZnO projected along [2$\bar{1}\bar{1}$0], displaying the ±(0001), ±(01$\bar{1}$1), and ±(0$\bar{1}$11) polar surfaces. (c) Model showing the formation of a nanospring by spiral coiling of a polar-surface-dominated nanobelt.

with a circular shape. The single-crystal structure referred to here means a complete nanoring that is made of a single-crystalline ribbon bent evenly at the curvature of the nanoring. The ZnO nanoring was made by coaxial, uniradius, epitaxial coiling of a nanobelt; sintering at high temperature made it a single crystal.

A Superlattice-Structured Nanohelix

By controlling the temperature ramping rate and steps, we have synthesized a superlattice-structured nanohelix of ZnO (Figures 3a and 3b).[18] High-resolution TEM revealed that the curly nanobelt has a superlattice structure with a periodic alternating arrangement of two types of stripes (Figure 3c) oriented epitaxially in the following orientations: stripe I has a growth direction of [1$\bar{1}$00], with top and bottom surfaces ±(0001) (polar surfaces); stripe II has a growth direction of [2$\bar{1}\bar{1}$2], with top and bottom surfaces ±(01$\bar{1}$0) (nonpolar surfaces). The corresponding electron diffraction pattern of the nanobelt shows that the growth directions of the two types of stripes have a small rotation of $\alpha \approx 4°$, indicating that the adjacent stripes rotate in the plane of the nanobelt at the same angle when forming the superlattice.

The formation of the nanohelix is a rigid structural alteration caused by the alternating stripes in the superlattice, and the formation of a superlattice is likely to be a polar-charge-induced structural transformation (see the inset in Figure 3c). As can be seen in Figure 2, the existence of the polar surfaces results in the formation of ZnO nanosprings and nanorings. If the width of the nanobelt is rather large, the electrostatic energy of the polar surfaces diverges with length. A possible way of reducing the electrostatic energy is to transform the polar surface into a nonpolar surface by introducing an orientation twisting between the stripes that compose the nanobelt. Provided that the interface mismatch energy is reasonably low, this will cause the formation of superlattice-structured stripes that are nearly parallel to the growth direction of the nanobelt. The width of the nanobelt increases after the structural transformation from a single-crystal, *c*-plane-dominated, stiff nanoribbon into a superlattice-structured, flexible nanobelt; the stripes are not exactly parallel to the growth direction of the nanobelt, and a small in-plane rotation angle exists between the growth directions of the two adjacent stripes, inducing the geometrical curvature required for rigidly twisting its shape. The polar charges remaining on the surfaces of stripe I also help to bend the nanobelt into a ring structure, especially with a decrease in the nanobelt thickness. Thus, the accumulation of rigid structural rotations or twists across the width of the superlattice nanobelt, accompanied by continuous growth of the stripes along the length of the nanobelt, results in the formation of a helical structure, which could be left-handed or right-handed. The winding of the nanobelt is terminated after the nanobelt fully transforms from a partial polar-surface-dominated and superlattice-structured nano-object into a single-crystal nanoribbon dominated by its nonpolar surface, which is likely to be caused by a change in growth kinetics. Such a nanohelix exhibits superelasticity, and it can be extended elastically to the theoretical limit.[19]

Nanomanufacturing of Aligned Nanowires

Growth of patterned and aligned 1D nanostructures is important for applications in sensing, optoelectronics, and field emission. Aligned growth of ZnO nanorods has been successfully achieved on a solid substrate using the vapor–liquid–solid (VLS) process with gold[20] and tin[21] as catalysts, in which the catalyst initiates and guides the growth, and the epitaxial orientation relationship between the nanorods and the substrate leads to the aligned growth (Figure 4a).[22–24]

The synthesis process involves three main steps. The hexagonally patterned ZnO nanorod arrays are grown on a single-crystal Al_2O_3 substrate on which patterned Au catalyst particles are dispersed. For the synthesis, first, a two-dimensional, large-area, self-assembled, and ordered monolayer of submicron polystyrene spheres is prepared on a single-crystal Al_2O_3/GaN substrate. Second, a thin layer of gold particles is deposited onto the self-assembled monolayer, and the polystyrene spheres are etched away, leaving a patterned gold catalyst array. Finally, nanowires are grown on the substrate using the VLS process.

In VLS growth, it may be assumed that nanowires will grow as long as the catalysts are supplied and the temperature is adequate. We have, however, shown that oxygen partial pressure in the chamber plays a key role in determining the quality of the aligned ZnO nanowires.[25] A "phase diagram" has been developed between the oxygen partial pressure and the growth chamber pressure for synthesizing high-quality aligned ZnO nanowires on a GaN substrate (Figure 4b).[25] Nanowires can only grow under the conditions defined by the red zone in the plot. This result provides a road map for large-scale,

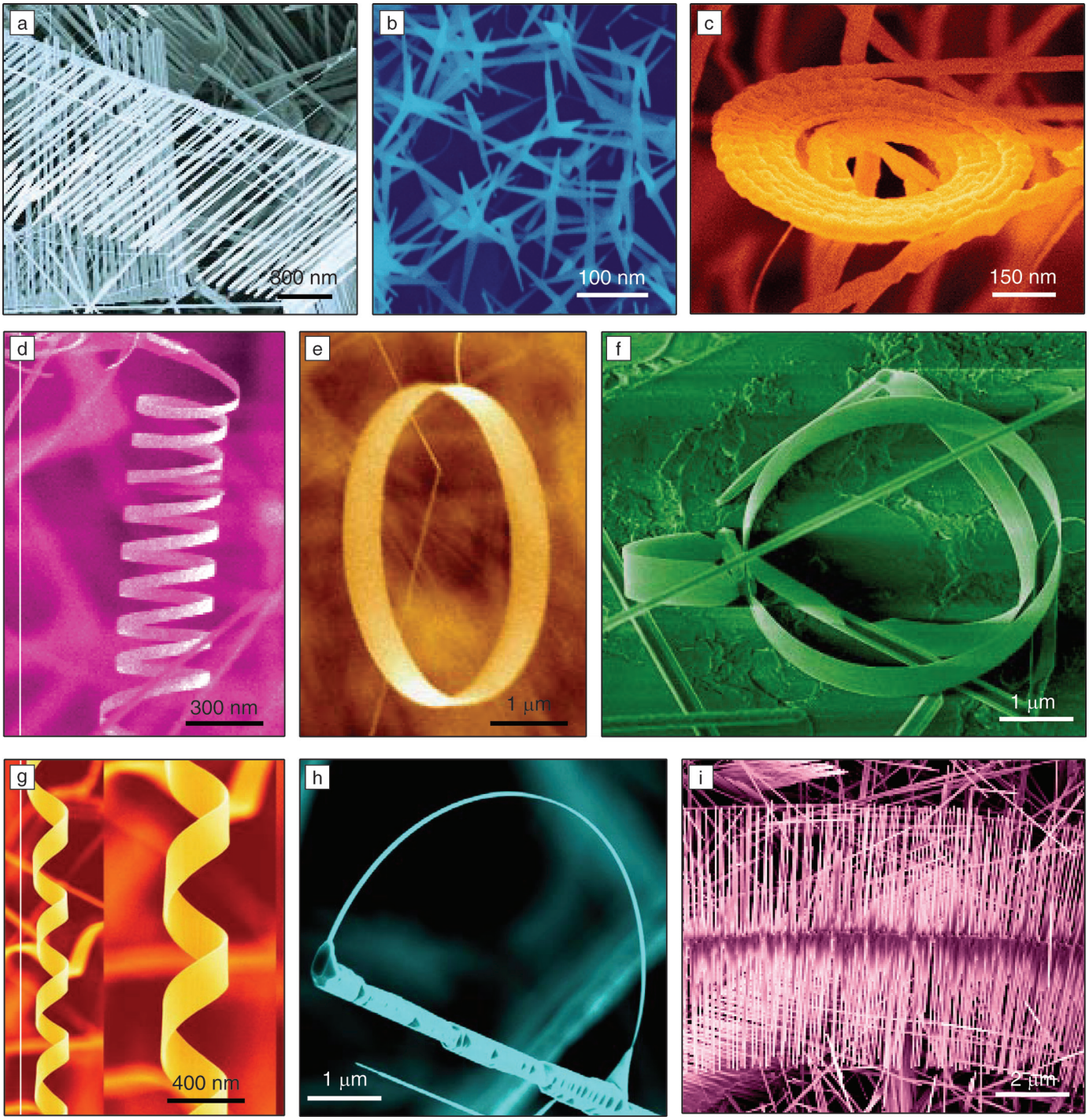

Figure 2. A collection of ZnO nanostructures resulting from polar-surface-induced growth phenomena. (a) Nanocombs/nanosaws,[37] (b) nano-tetrapoles,[41] (c) nanospirals,[11] (d) nanosprings,[11] (e) nanorings,[12] (f) a combination of nanoring and nanobow,[42] (g) nanohelices,[18] (h) nanobows,[43] and (i) double-sided nanosaws.[44]

controlled synthesis of aligned ZnO nanowires with the potential to meet the needs of practical applications such as nanogenerators and field emission. The chemical process involved in the growth of nanowires is also systematically elaborated based on experimental data obtained under different conditions. A systematic study has also been carried out for producing pure nanowires, nanobelts, or nanosaws of CdSe, aiming at exploring a possible path for nanomanufacturing.[26]

Furthermore, the growth morphology of the nanowires can be drastically changed by varying the experimental conditions. Figures 4c and 4d show ZnO nanowires synthesized through a thermal evaporation process in a horizontal tube

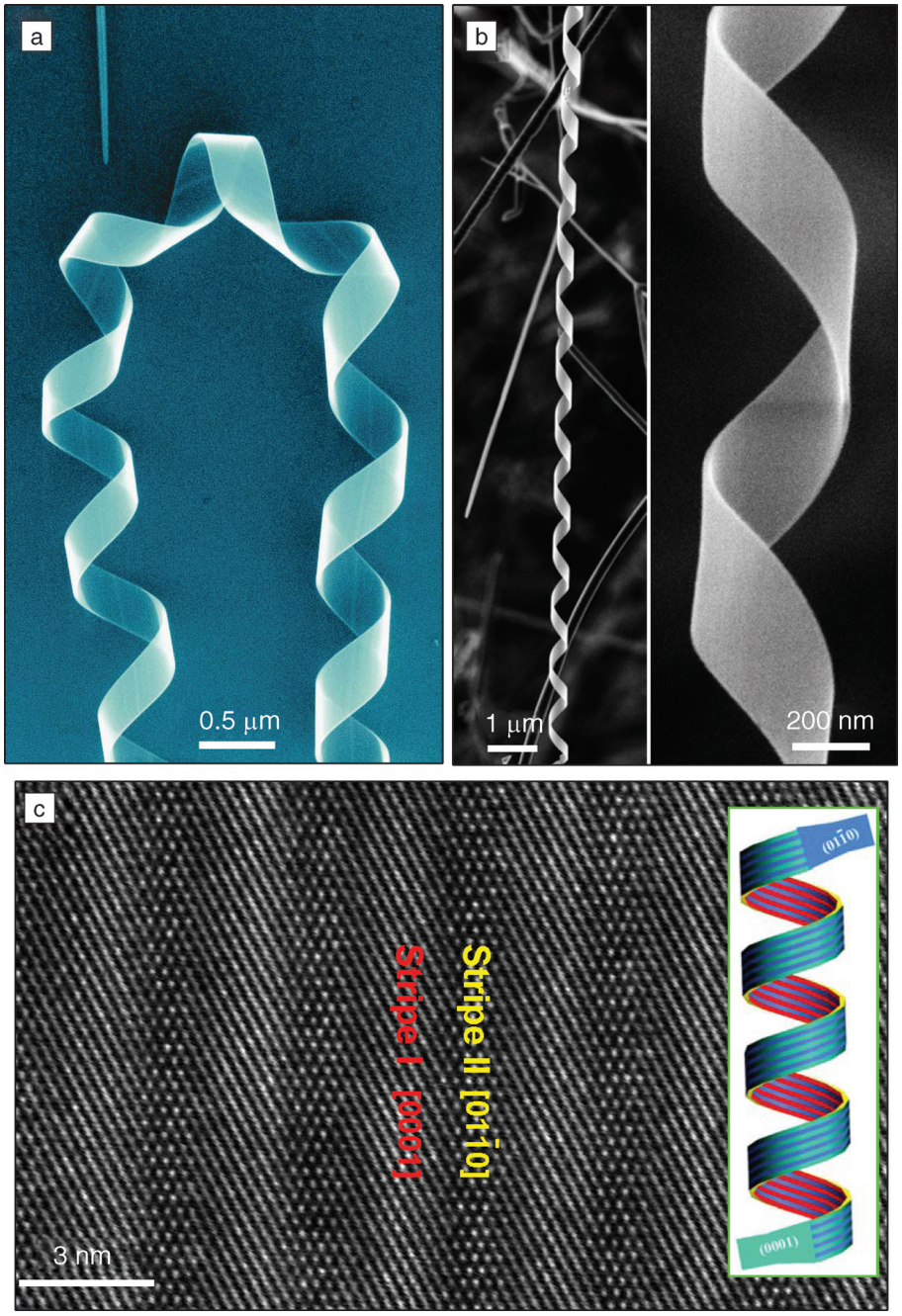

Figure 3. Formation of ZnO nanohelices. (a) Low-magnification and (b) high-magnification scanning electron micrographs of nanohelices synthesized by a solid–vapor process. (c) High-resolution transmission electron micrograph of a superlattice-structured nanohelix, showing coherent, periodically arranged stripes. The inset shows a model of the formation and structure of the nanohelix.[18]

furnace. Commercial grade ZnO powder was placed in the center of a single-zone tube furnace and evacuated for several hours to purge oxygen in the chamber. A polycrystalline alumina substrate was used for growing the nanostructures. The morphology of the as-synthesized nanowires is unique.

Mechanical Properties

Atomic force microscopy (AFM) is a common technique for characterizing the mechanical behavior of nanostructures.[27,28] One of the most important strategies is to use an AFM tip to deform a nanowire supported at both ends by pushing the nanowire at its middle point. Quantifying the middle-point force-displacement curve gives the elastic modulus. The accuracy of this measurement is, however, limited by the size of the tip and the accuracy of positioning the AFM tip right at the center of the 1D nanostructure due to the unavoidable hysteresis of the piezoceramic actuator of the AFM cantilever. We have demonstrated a new approach for quantifying the elastic deformation behavior of a nanowire by fitting the image profile measured using AFM in contact mode along the entire length of a suspended nanobelt/nanowire/nanotube under different load forces (Figure 5a).[29] The profile images of the nanobelt recorded the deformation of all the points along the length under different applied forces (Figure 5b). One profile can contain up to 650 points, and each point on the suspended portion of nanobelt in the images can be regarded as a mechanical measurement. Consistently fitting the measured deformation profiles can uniquely determine if the measured data are best fit by the free-free beam model (FFBM) rather than the clamped-clamped beam model (CCBM) (Figure 5c). It also eliminates the uncertainty in defining the central point of the suspended beam, thus greatly increasing the precision and reliability of the measurement for elastic modulus.

Piezo-Resonator

Bulk acoustic resonators have shown a great deal of promise for applications as high-performance frequency control devices in wireless systems such as cell phones, navigation systems, satellite communications, and other forms of data communication. These devices consist of a thin piezoelectric film sandwiched between two electrodes. An rf signal applied through the thickness of the film produces mechanical motion, and fundamental resonance occurs when the film thickness equals one-half of the wavelength of the input signal. Piezoelectric nanobelts of ZnO can be effective piezo-resonators due to their high uniformity and dislocation-free structure. Using a single belt, we have demonstrated a bulk acoustic resonator (Figure 6a).[30] By measuring the impedance response across the nanobelt (Figure 6b), the resonance frequency can be identified in both the phase and amplitude images (Figure 6c). The fabricated device was characterized using vector network analysis, and both the first and third harmonics of resonance were observed at approximately 247 MHz and 754 MHz, respectively. A 1D Krimholt–Leedom–Matthaei (KLM) model was utilized to predict the resonant frequency of the device and confirm the observed behavior (Figure 6c).

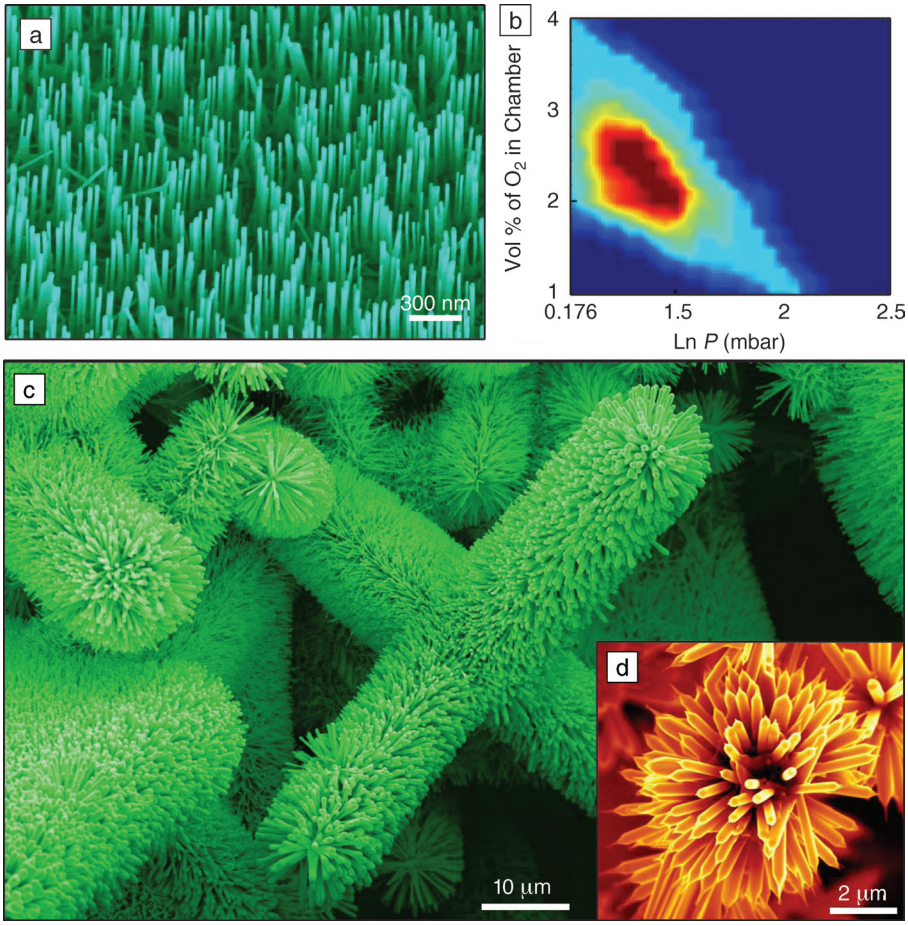

Figure 4. Growth of patterned and aligned ZnO nanowires. (a) Aligned ZnO nanowires grown on a single-crystal alumina substrate with a honeycomb pattern defined by the catalyst mask. (b) A "phase diagram" between the oxygen partial pressure and total pressure in the growth chamber for the growth of the nanowires.[22,25] (c),(d) Scanning electron micrographs of as-synthesized nanowire assemblies of ZnO.

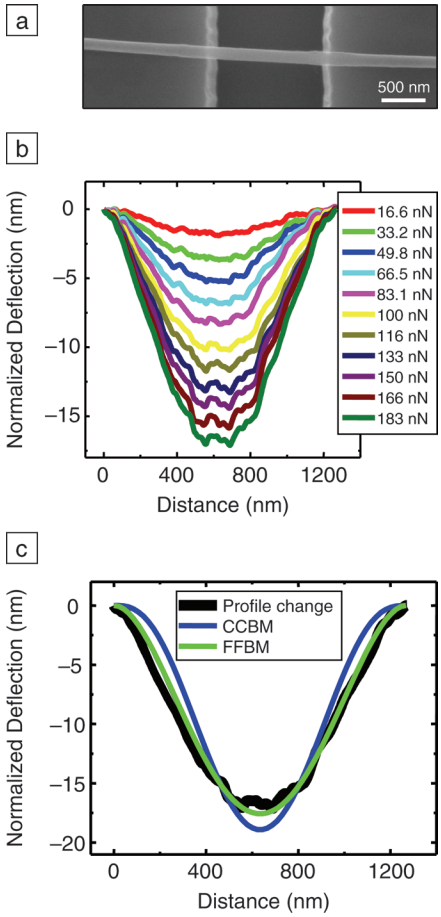

Figure 5. (a) Scanning electron micrograph of a nanobelt bridged over a trench. (b) The normalized atomic force microscopy profile along the nanotube under different loads after removing the surface roughness. (c) A quantitative fitting of the shape of the curve using the calculated results of the free-free beam model (FFBM) and the clamped-clamped beam model (CCBM). The data are best fitted by the FFBM model.[29]

Piezoelectric Nanogenerator

Wireless devices may allow *in situ*, real-time biomedical monitoring and detection, but such devices still require a power source. Ideally, such devices should be self-powered rather than use a battery. The body provides numerous potential power sources—mechanical energy, vibrational energy, chemical energy (glucose), and hydraulic energy, but the challenge is their efficient conversion into electric energy. If accomplished on the nanoscale, such power sources could greatly reduce the size of integrated nanosystems for optoelectronics,[31] biosensors,[32] resonators,[33] and other applications. We have demonstrated an approach for converting mechanical energy into electric power using aligned ZnO nanowires.[34]

The study was based on aligned ZnO nanowires grown on a *c*-plane oriented α-Al_2O_3 substrate covered by a layer of ZnO film (Figure 7a).[23] The measurements were performed by AFM using a Si tip coated with a Pt film. The output voltage was continuously monitored as the tip scanned over the nanowires (note the defined polarity of the voltage signal in Figure 7b). No external voltage was applied in any stage of the experiment.

Experimentally, both the topography (feedback signal from the scanner) and the corresponding output voltage (V_L) images across the load were recorded simultaneously when the AFM tip was scanned over the aligned nanowire arrays. In the voltage output image (Figure 7c), many sharp output peaks (like discharge peaks) were observed, which are typically ~4–50 times higher than the noise level. The location of the voltage peak is directly registered at the site of the nanowire.

The physical principle for creating, separating, and preserving the piezoelectric charges in the nanowire is a coupling of piezoelectric and semiconducting properties, as explained in detail below.[34,35] For a vertical, straight ZnO nanowire (Figure 8a), the deflection of the nanowire by an AFM tip creates a strain field, with the outer surface being stretched (positive strain) and inner surface compressed (negative strain) (Figure 8b). An electric field E_z along the nanowire (z direction) is then created inside the nanowire volume through the piezoelectric effect, $E_z = \varepsilon_z/d$, where d is the piezoelectric coefficient[36] along the nanowire direction that is normally the positive *c*-axis of ZnO, with the Zn atomic layer being the front terminating layer.[37] The piezoelectric field direction is closely parallel to the z-axis

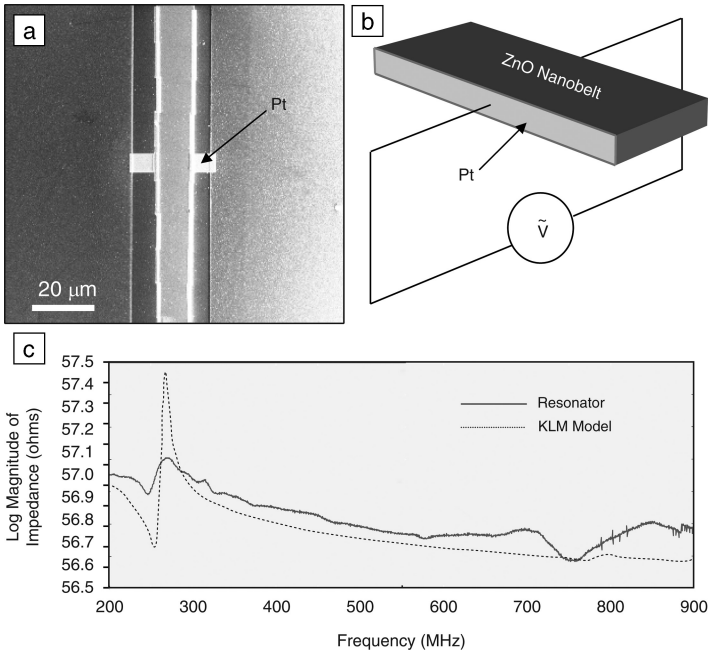

Figure 6. (a) Scanning electron micrograph of a bulk acoustic resonator; the vertical gray bar is the nanobelt and the horizontal white bar is Pt. (b) Schematic illustration of the piezo-resonator circuit design. (c) Plot of the magnitude of the absolute value of the measured impedance (|Z|) and the predicted traces from the applied Krimholt–Leedom–Matthaei (KLM) model, confirming the results from the working device.[30]

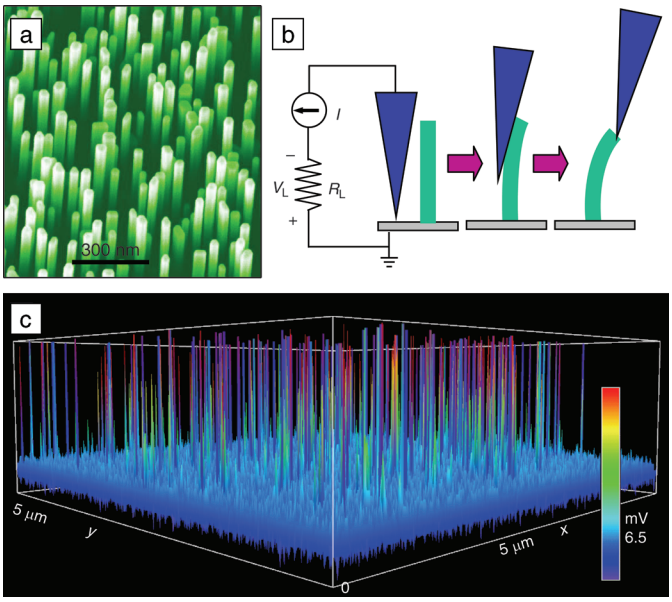

Figure 7. (a) Scanning electron micrographs of aligned ZnO nanowires grown on an α-Al_2O_3 substrate. (b) Experimental setup and procedures for generating electricity by deforming a piezoelectric nanowire using a conductive atomic force microscope tip. The root of the nanowire is grounded, and an external load of $R_L = 500\ M\Omega$ is applied, which is much larger than the inner resistance R_i of the nanowire. The AFM tip scans across the nanowire arrays in contact mode. (c) Output voltage image of the nanowire arrays when the AFM tip scans across the nanowire arrays. The discharging process is so quick that each discharge event is characterized by only a couple of data points. This makes it difficult to display the data with a color spectrum.

(nanowire direction) at the outer surface and anti-parallel to the *z*-axis at the inner surface (Figure 8c). Under the first-order approximation, across the width of the nanowire at the top end, the electric potential distribution from the compressed to the stretched side surface is approximately between V_s^- (negative) to V_s^+ (positive), where the subscripts stand for surface. The electrode at the base of the nanowire is grounded. Note that V_s^+ and V_s^- are the voltages produced by the piezoelectric effect. The potential is created by the relative displacement of the Zn^{2+} cations with respect to the O^{2-} anions due to the piezoelectric effect in the wurtzite crystal structure; thus, these ionic charges cannot freely move nor recombine without releasing the strain (Figure 8d). The potential difference is maintained as long as the deformation is in place, and no foreign free charges (such as from the metal contacts) are injected.

We now consider the discharge process. In the first step, the AFM conductive tip that induces the deformation is in contact with the stretched surface of positive potential V_s^+ (Figures 8d and 8e). The Pt metal tip has a potential V_m of nearly zero, so the metal tip–ZnO interface is negatively biased for $\Delta V = V_m - V_s^+ < 0$. For the *n*-type semiconductor characteristic of the as-synthesized ZnO nanowires, the Pt metal–ZnO semiconductor interface in this case is a reverse-biased Schottky diode (Figure 8e), and little current flows across the interface. In the second step, when the AFM tip is in contact with the compressed side of the nanowire (Figure 8f), the metal tip–ZnO interface is positively biased for $\Delta V = V_L = V_m - V_s^- > 0$; V_L is the voltage across the external load. The metal–semiconductor interface in this case is a positively (forward) biased Schottky diode, and it produces a sudden increase in the output electric current. The current is the result of ΔV-driven flow of electrons from the semiconductor ZnO nanowire to the metal tip. The flow of the free electrons from the loop through the nanowire to the tip will neutralize the ionic charges distributed in the volume of the nanowire and thus reduce the magnitudes of the potential V_s^- and V_s^+.

The principle and technology demonstrated here have the potential of converting mechanical movement energy (body movement, muscle stretching, blood pressure), vibration energy (acoustic/ultrasonic waves),[38] and hydraulic energy (body fluid flow, blood flow, contraction of blood vessels, dynamic fluid flow in nature) into electric energy that may be sufficient for self-powering nanodevices and nanosystems. The technology could have

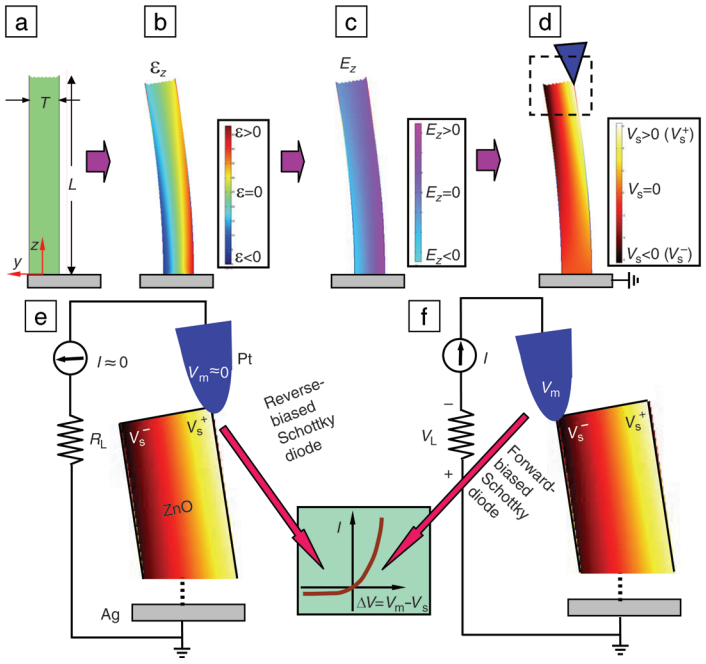

Figure 8. Physical principle of the observed power generation process of a piezoelectric ZnO nanowire, showing a unique coupling of piezoelectric and semiconducting properties. (a) Schematic illustration of a nanowire and the coordination system. T is thickness and L is length. (b) Longitudinal strain ε_z distribution in the nanowire after being deflected by an AFM tip from the side. Data simulated by FEMLAB for a ZnO nanowire 1 μm long with an aspect ratio of 10. (c) Corresponding longitudinal piezoelectric-induced electric field E_z distribution in the nanowire. (d) Potential distribution in the nanowire as a result of the piezoelectric effect. Dashed box indicates the area shown in detail in (e) and (f). Metal (e) and semiconductor (f) contacts between the AFM tip and the semiconductor ZnO nanowire at two reversed local contact potentials (positive and negative), showing reverse-biased and forward-biased Schottky rectifying behavior, respectively (see text for details). It is this oppositely biased Schottky barrier across the nanowire that makes it possible to preserve the piezoelectric charges and later produce the discharge output. Inset is a typical I–V characteristic of a metal semiconductor (n-type) Schottky barrier. The process in (e) builds up the potential; the process in (f) discharges the potential.[34,35]

important applications in wireless self-powered nanodevices by harvesting energy from the environment. It also provides a method for indirectly charging a battery. It is also possible to fabricate a large-power-output electric generator by using arrays of ZnO wires/belts, which can be grown on substrates such as metal foils, flexible organic plastic substrates,[38] ceramic substrates (such as alumina), and compound semiconductors (such as GaN and AlN). The nanogenerator could be the basis for exploring new self-powering technologies for *in situ*, real-time, and implantable biosensing, biomedical monitoring, and biodetection. It could also have the potential of solving key energy requirements for remote sensing and actuating.

Summary

Zinc oxide has three key properties. First, it is a semiconductor, with a direct, wide bandgap (3.37 eV) and a large excitation binding energy (60 meV). It is an important functional oxide, exhibiting near-UV emission and transparent conductivity. Second, due to its non-central symmetry, it is piezoelectric, which is a key phenomenon in building electromechanical coupled sensors and transducers. Finally, ZnO is bio-safe and biocompatible,[39] and it can be used for biomedical applications without coating. With these three distinct characteristics, in addition to the unique polar-surface-dominated growth, ZnO has great potential in future research and applications. The novel nanostructures that can be grown for ZnO provide the fundamental units for constructing and assembling advanced nanodevices. The principle demonstrated in this article for the nanogenerator is the fundamental of nano-piezotronics, a new field that utilizes piezoelectric–semiconducting coupled properties for designing and fabricating electronic devices and components such as piezoelectric field-effect transistors,[40] piezoelectric field gated diodes,[45] and force/pressure sensors.[40]

Acknowledgments

Thanks to Y. Ding, P.X. Gao, J.H. Song, X.D. Wang, R.S. Yang, C.S. Lao, W.L. Hughes, B. Buchine, W.J. Mai, X.Y. Kong, J. Liu, C. Ma, Y. Dai, and Y. Zhang for their contributions to the work reviewed in this article. We acknowledge generous support from DARPA, NSF, NASA, and NIH.

References

1. Z.W. Pan, Z.R. Dai, and Z.L. Wang, *Science* **291** (2001) p. 1947.
2. Z.L. Wang, *J. Phys.: Condens. Matter* **16** (2004) p. 829.
3. M.S. Arnold, P. Avouris, and Z.L. Wang, *J. Phys. Chem. B* **107** (2002) p. 659.
4. E. Comini, G. Faglia, G. Sberveglieri, Z.W. Pan, and Z.L. Wang, *Appl. Phys. Lett.* **81** (2002) p. 1869.
5. X.D. Bai, P.X. Gao, Z.L. Wang, and E.G. Wang, *Appl. Phys. Lett.* **82** (2003) p. 4806.
6. W. Hughes and Z.L. Wang, *Appl. Phys. Lett.* **82** (2003) p. 2886.
7. L. Shi, Q. Hao, C. Yu, D. Kim, N. Mingo, X.Y. Kong, and Z.L. Wang, *Appl. Phys. Lett.* **84** (2004) p. 2638.
8. S.C. Minne, S.R. Manalis, and C.F. Quate, *Appl. Phys. Lett.* **67** (1995) p. 3918.
9. See the special issue on transparent conducting oxides, *MRS Bull.* **25** (August 2000).
10. C.R. Gorla, N.W. Emanetoglu, S. Liang, W.E. Mayo, Y. Lu, M. Wraback, and H. Shen, *J. Appl. Phys.* **85** (1999) p. 2595.
11. X.Y. Kong and Z.L. Wang, *Nano Lett.* **3** (2003) p. 1625.
12. X.Y. Kong, Y. Ding, R. Yang, and Z.L. Wang, *Science* **303** (2004) p. 1348.
13. Z.L. Wang, X.Y. Kong, Y. Ding, P. X. Gao, W. Hughes, R.S. Yang, and Y. Zhang, *Adv. Funct. Mater.* **14** (2004) p. 944.
14. Z.L. Wang, *Mater. Today* **7** (June 2004) p. 26.
15. P.X. Gao and Z.L. Wang, *Small* **1** (2005) p. 945.
16. W.L. Hughes and Z.L. Wang, *Appl. Phys. Lett.* **86** 043106 (2005).
17. Y. Ding, X.Y. Kong, and Z.L. Wang, *Phys. Rev. B* **70** 235408 (2004).
18. P.X. Gao, Y. Ding, W.J. Mai, W.L. Hughes, C.S. Lao, and Z.L. Wang, *Science* **309** (2005) p. 1700.
19. P.X. Gao, W.J. Mai, and Z.L. Wang, *Nano Lett.* **6** (2006) p. 2536.
20. P.D. Yang, H.Q. Yan, S. Mao, R. Russo, J. Johnson, R. Saykally, N. Morris, J. Pham, R.R. He, and H.J. Choi, *Adv. Funct. Mater.* **12** (2002) p. 323.
21. P.X. Gao, Y. Ding, and Z.L. Wang, *Nano Lett.* **3** (2003) p. 1315.
22. X.D. Wang, C.J. Summers, and Z.L. Wang, *Nano Lett.* **3** (2004) p. 423.
23. X.D. Wang, J.H. Song, C.J. Summers, J.H. Ryou, P. Li, R.D. Dupuis, and Z.L. Wang, *J. Phys. Chem. B* **110** (2006) p. 7720.
24. X.D. Wang, J.H. Song, P. Li, J.H. Ryou, R.D. Dupuis, C.J. Summers, and Z.L. Wang, *J. Am. Chem. Soc.* **127** (2005) p. 7920.
25. J.H. Song, X.D. Wang, E. Riedo, and Z.L. Wang, *J. Phys. Chem. B* **109** (2005) p. 9869.
26. C. Ma and Z.L. Wang, *Adv. Mater.* **17** (2005) p. 1.
27. E.W. Wong, P.E. Sheehan, and C.M. Lieber, *Science* **277** (1997) p. 1971.

28. J.P. Salvetat, G.A.D. Briggs, J.M. Bonard, R.R. Bacsa, A.J. Kulik, T. Stockli, N.A. Burnham, and L. Forro, *Phys. Rev. Lett.* **82** (1999) p. 944.
29. W.J. Mai and Z.L. Wang, *Appl. Phys. Lett.* **89** 073112 (2006).
30. B.A. Buchine, W.L. Hughes, F.L. Degertekin, and Z.L. Wang, *Nano Lett.* **6** (2006) p. 1155.
31. X.F. Duan, Y. Huang, R. Agarwal, and C.M. Lieber, *Nature* **421** (2003) p. 241.
32. G.F. Zheng, F. Patolsky, Y. Cui, W.U. Wang, and C.M. Lieber, *Nature Biotechnol.* **23** (2005) p. 1294.
33. X.D. Bai, P.X. Gao, Z.L. Wang, and E.G. Wang, *Appl. Phys. Lett.* **82** (2003) p. 4806.
34. Z.L. Wang and J.H. Song, *Science* **312** (2006) p. 242.
35. J.H. Song, J. Zhou, and Z.L. Wang, *Nano Lett.* **6** (2006) p. 1656.
36. M.H. Zhao, Z.L. Wang, and S.X. Mao, *Nano Lett.* **4** (2004) p. 587.
37. Z.L. Wang, X.Y. Kong, and J.M. Zuo, *Phys. Rev. Lett.* **91** 185502 (2003).
38. P.X. Gao, J.H. Song, J. Liu, and Z.L. Wang, U.S. patent pending (2006).
39. J. Zhou, N.S. Xu, and Z.L. Wang, *Adv. Mater.* **18** (2006) p. 2432.
40. X.D. Wang, J. Zhou, J.H. Song, J. Liu, N.S. Xu, and Z.L. Wang, *Nano Lett.* **6** (2006) p. 2768.
41. Y. Dai, Y. Zhang, and Z.L. Wang, *Solid State Commun.* **126** (2003) p. 629.
42. P.X. Gao and Z.L. Wang, *J. Appl. Phys.* **97** 044304 (2005).
43. W.L. Hughes, and Z.L. Wang, *J. Am. Chem. Soc.* **126** (2004) p. 6703.
44. C.S. Lao, P.X. Gao, R.S. Yang, Y. Zhang, Y. Dai, and Z.L. Wang, *Chem. Phys. Lett.* **417** (2005) p. 359.
45. J.H. He, C.H. Hsin, L.J. Chen, and Z.L. Wang, *Adv. Mater*. (2006) in press. □